The role of hafnium acetylacetonate buffer layer on the performance of lead halide perovskite solar cells derived from dehydrated lead acetate as Pb source

Cite as: AIP Advances **10**, 075006 (2020); https://doi.org/10.1063/5.0012646
Submitted: 04 May 2020 . Accepted: 13 June 2020 . Published Online: 02 July 2020

D. M. Sanni, E. Ntsoenzok, E. Saintaimé, S. A. Adeniji, O. V. Oyelade, R. K. Koech, D. I. Amune, and A. Bello

The role of hafnium acetylacetonate buffer layer on the performance of lead halide perovskite solar cells derived from dehydrated lead acetate as Pb source

Cite as: AIP Advances 10, 075006 (2020); doi: 10.1063/5.0012646
Submitted: 4 May 2020 • Accepted: 13 June 2020 •
Published Online: 2 July 2020

D. M. Sanni,[1,2,a] E. Ntsoenzok,[3,4] E. Saintaimé,[3] S. A. Adeniji,[1,5] O. V. Oyelade,[1,6] R. K. Koech,[4,7] D. I. Amune,[4] and A. Bello[1,4]

AFFILIATIONS

[1]Department of Theoretical and Applied Physics, African University of Science and Technology (AUST), P.M.B. 681 Garki, Abuja, Nigeria
[2]Department of Physics, Federal University, P.M.B. 5001, Dutsin-Ma, Katsina State, Nigeria
[3]CEMHTI-CNRS Site Cyclotron, 3A rue de la férollerie, 45071 Orléans, France
[4]Department of Material Science and Engineering African University of Science and Technology (AUST), P.M.B. 681 Garki, Abuja, Nigeria
[5]Faculty of Natural and Applied Sciences Nile University of Nigeria, Plot 681, Cadastral Zone C-OO, Research and Institution Area Jabi, Abuja 900001, Nigeria
[6]Department of Physics, Bingham University, Km. 26 Abuja-Keffi Express Way, P.M.B. 005, Karu, Nasarawa State, Nigeria
[7]Moi University, P.O. Box 3900-30100, Eldoret, Kenya

[a]**Author to whom correspondence should be addressed:** dahirusanni@gmail.com

ABSTRACT

In this research, we demonstrated the use of hafnium acetylacetonate (Hfaca) dissolved in ethanol as a buffer layer for perovskite solar cells from non-halide Pb (dehydrated lead acetate) source material. The inverted p-i-n planar heterojunction structure was employed in this work. A one step spin-coating method was used in depositing the perovskite solution before thermal annealing at 90 °C for 5 min to form the perovskite film. Hfaca has been previously used as a buffer layer, but the optimal concentration has not been reported. The optimum concentration of Hfaca was found to be 1.0 mg/ml, resulting in a power conversion efficiency (PCE) of 12.23% corresponding to more than 30% improvement when compared to the control device (phenyl-C_{61}-butyric acid methyl ester/Ag) without Hfaca, which has a PCE of 8.89%. Hfaca as a buffer layer leads to superior stability, retaining about 90% of its original PCE values after 15 days of storage in a glove box, compared to the control device, which retains 70% of the initial PCE value under the same storage.

I. INTRODUCTION

Organic–inorganic lead halide perovskites have attracted growing research interest over the last decade as the most promising materials for photovoltaic applications. This is because of their exceptional advantages such as light-weight, solution processability, tunable bandgap, high diffusion length, high absorption coefficient, flexible manufacturing process, etc.[1–4] Organic–inorganic lead halide perovskite solar cells (PSCs) have recorded significant success since their first application by Kojima and co-workers, with a power conversion efficiency (PCE) of 3.8% compared to the present record of 25.2%.[5,6] Moreover, due to their unique properties, several PSC device architectures have been reported over the past few years, such as mesoporous structures and planar architectures; the planar

heterojunction architecture can also either be n-i-p or inverted p-i-n. To achieve a high PCE in PSCs, a combination of high-quality photoactive layers and interface engineering of charge transport layers is required to enhance the transportation of photo-generated charge carriers to their respective electrodes.[7–9] Both the planar heterojunction and mesoporous architectures have recorded a high PCE.[10–13] The mesoporous architecture has some limitations owing to the complicated architecture, complex charge transport paths, tedious processes, and high processing temperature of over 450 °C,[14] which hinder its application on a flexible substrate and normal glass.[15] Planar heterojunction architectures have a simpler structure and a low processing temperature of less than 100 °C;[16] this makes the architecture an attractive option to PSC researchers in recent times. However, in the absence of a mesoporous scaffold, regular planar n-i-p PSCs experience a great hysteresis in *J*–*V* measurements under forward and reverse scanning directions due to ion migration and trapping of surface states.[17–20] However, the inverted planar heterojunction p-i-n PSC architecture eliminates the hysteresis effect during J–V curve measurements in different scanning directions.[21] Inverted planar heterojunction PSCs are composed of transparent conductive oxide [e.g., indium doped tin oxide (ITO)]/hole transport layer [e.g., poly (3,4-ethylene dioxythiophene): poly (styrene sulfonate) (PEDOT:PSS)]/perovskite layer/electron transport layer [e.g., phenyl-C_{61}-butyric acid methyl ester (PCBM)]/metal electrode.[16,22] This type of architecture requires a buffer layer such as bathocuproine (BCP),[23] zirconium acetylacetonate,[24] titanium acetylacetonate,[25] or hafnium acetylacetonate (Hfaca)[26] between the electron transport layer and the metal electrode to improve the performance of the device.

Yu *et al.* employed hafnium acetylacetonate (Hfaca) as a buffer layer for polymer solar cells, which improved the PCE by 26%. However, they did not report the optimum concentration of the buffer layer.[26] Chen *et al.* reported that employing metal acetylacetonate (i.e., zirconium acetylacetonate, titanium acetylacetonate, and hafnium acetylacetonate) as a cathode buffer layer helped improve the performance of inverted PSCs by 34%.[25] The degradation of perovskite devices comes mainly from the decomposition of the $CH_3NH_3PbI_3$ layer in the presence of moisture, temperature, chemicals, and UV light.[27] The metal acetylacetonate series, of which Hfaca is a member, have been reported to have high pyrolysis temperature, high hydrolysis threshold, and insensitivity toward water and chemicals due to a strong chelate bond.[28] These properties of Hfaca helps improve the stability of devices with an Hfaca buffer layer compared to devices without an Hfaca buffer layer. The availability and ease of processing without further annealing make it a good candidate for cost-effective large scale production. This research seeks to address the effect of optimal solution concentration of the Hfaca buffer layer.

In this research, we investigated the optimal solution concentration of Hfaca as the cathode buffer layer by preparing different solution concentrations of Hfaca in ethanol. The device structure adopted for this study is an inverted planar (p-i-n) PSC structure of ITO/PEDOT:PSS/$CH_3NH_3PbI_3$/PCBM/Hfaca/Ag, as shown in Fig. 1(a). The methylammonium lead iodide perovskite film ($CH_3NH_3PbI_3$) used in this study was obtained by the reaction of methylammonium iodide (MAI) with dehydrated lead acetate [$Pb(Ac)_2$] [see Eq. (1)] with dimethylformamide (DMF) as the solvent,

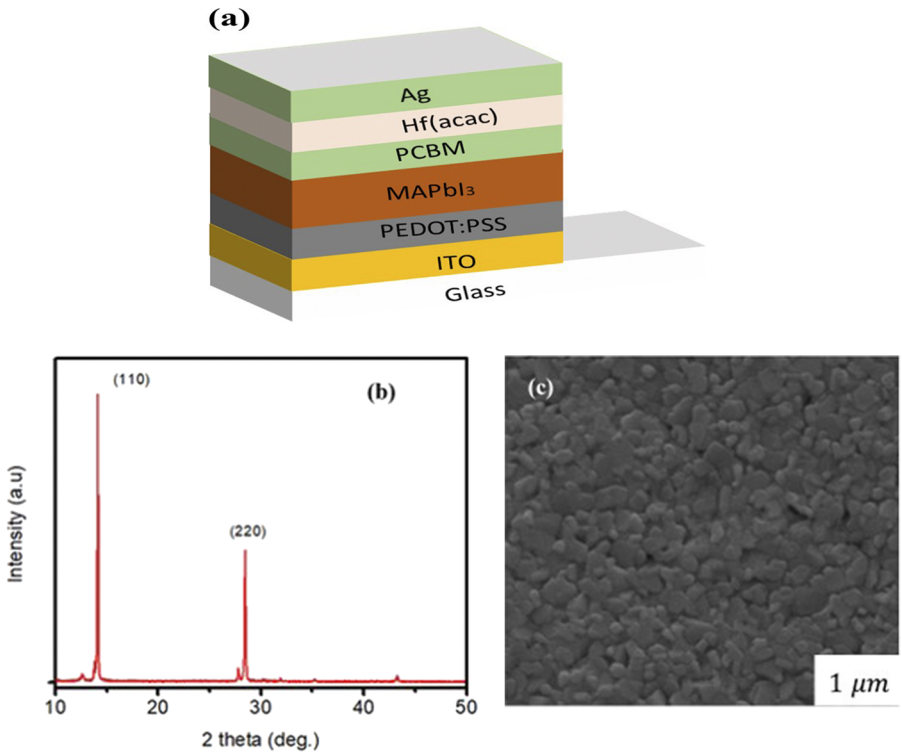

FIG. 1. (a) Schematic diagram of the inverted planar heterojunction perovskite solar cell architecture with Hfaca, (b) XRD patterns, and (c) the SEM picture of the perovskite film used in all the devices.

$$Pb(CH_3OO)_2 + 3CH_3NH_3I \rightarrow CH_3NH_3PbI_3 + 2CH_3NH_3COO\uparrow \text{ (Ref. 29)}. \quad (1)$$

II. MATERIALS AND EXPERIMENTAL METHODS

Lead acetate trihydrate ($PbAc_2{\cdot}3H_2O$) was obtained from Alfa Aesar, and methylammonium iodide (MAI) was supplied by Ossila. $PbAc_2{\cdot}3H_2O$ was heated in an oven at 81 °C for 23 h to obtain $Pb(Ac)_2$. 2.9 mmol of MAI and 0.9 mmol of $Pb(Ac)_2$ were dissolved in 1 ml of DMF to obtain the perovskite solution. PEDOT: PSS and PCBM were bought from Ossila, while hafnium acetylacetonate was obtained from Alfa Aesar.[16,22]

Patterned glass/ITO substrates were cleaned in a sonicator with detergent solution, deionized water, acetone, and isopropyl alcohol for 20 min, before drying the setup with flowing nitrogen gas. Finally, the substrates were transferred into ultraviolet-ozone (UVO) and kept for 18 min. The substrate has a dimension of 2.5 × 2.5 cm^2 with an active area of 0.2 cm^2. PEDOT: PSS solution was filtered through 0.45 μm filter PES purchased from Ossila, which is the hole transport layer (HTL); the filtrate of PEDOT:PSS was subsequently deposited onto the patterned glass/ITO via a spin-coating technique at the rate of 4×10^3 rpm for 60 s before thermal annealing immediately at 140 °C for 15 min. The perovskite solution was then deposited onto the HTL at a spin-coating rate of 4×10^3 rpm for 60 s followed by thermal annealing at 90 °C for 5 min to form the absorber layer. All the deposition processes were carried out in a nitrogen-filled glove box.[30]

20 mg of PCBM was dissolved in 1 ml of chlorobenzene solvent to obtain the solution for the electron transport layer (ETL), which was deposited on the $CH_3NH_3PbI_3$ layer at the rate of 1000 rpm for 30 s. In optimizing the Hfaca solution concentrations, four sets of devices were fabricated: three with Hfaca concentrations of 0.5 mg/ml, 1.0 mg/ml, and 1.5 mg/ml to serve as the buffer layer and a control cell without Hfaca. The three different solution concentrations of Hfaca were prepared by dissolving Hfaca powder in ethanol. The concentrations of Hfaca are 0.5 mg/ml, 1.0 mg/ml, and 1.5 mg/ml and are denoted as Hf1, Hf2, and Hf3, respectively. The Hfaca solutions were spin-coated onto the PCBM layer at 3000 rpm for 40 s, resulting in film thicknesses of 5.2 nm, 8.9 nm, and 11.7 nm respectively. Finally, the silver (Ag) electrode was thermally deposited on the Hfaca layer. The fabricated device is an inverted planar heterojunction solar cell with a typical architecture of glass/ITO/PEDOT:PSS/$CH_3NH_3PbI_3$/PCBM/Hfaca/Ag [see Fig. 1(a)].

The as-prepared perovskite films were characterized by scanning electron microscopy [SEM-XL30 Environmental FEG (FEI)] to study the surface morphology. The perovskite crystal formation was characterized by x-ray diffraction (XRD) using an anode tension of 40 kV and a filament current of 45 mA to produce copper $K\alpha$ radiation. A step-size of 0.01° was used for the evaluation. The crystallite size was calculated from the (110) of the $CH_3NH_3PbI_3$ peak using Scherrer's equation,

$$D = \frac{K\lambda}{\beta \cos\theta} \text{ (Ref. 31)}. \quad (2)$$

Here, β is the full width at half maximum (FWHM), θ is Bragg's angle in degrees, k = 0.9, λ is the x-ray wavelength in nm, and D is the crystallite size in nm.

The absorption spectra were characterized by a Cary 5000 UV/VIS photo spectrometer.

A surface profilometer was used to measure the film thickness of the Hfaca layers. Current density–voltage (J–V) parameters of the PSCs were evaluated with simulated AM 1.5 global solar irradiation (100 mW/cm^2) using a xenon-lamp solar simulator (Spectra-Physics, Oriel Instruments, USA).

III. RESULTS AND DISCUSSION

In this study, we used the same perovskite active layer for all the devices, and it was prepared by a single step spin coating technique, as explained in the experimental section. Figure 1(a) presents the schematic diagram of the PSC structure used for this study. Figures 1(b) and 1(c) present the XRD patterns and the SEM pictures of the perovskite film, respectively. The XRD result shows a prominent diffraction peak at 14.24 and 28.48, which correspond to peak (110) and peak (220) lattice planes of the $CH_3NH_3PI_3$ phase, respectively. Scherrer's equation was used to calculate the crystallite size from the XRD patterns. Peak (110), shown in Fig. 1(b), was used to calculate the FWHM. The values of the FWHM and the corresponding crystallite size of the perovskite films are 0.1709 nm and 96.35 nm, respectively. The SEM image of the perovskite film reveals uniform densely packed grains over the entire area with few pinholes or pores.

The absorbance and transmittance properties of the perovskite film used for this research were determined by UV–Vis spectroscopy. The absorbance of the perovskite film with PCBM deposited on it was compared with that deposited with different concentrations of Hfaca layers, as shown in Fig. 2(a). We observed no major difference between the absorbance of the perovskite film deposited with Hfaca and that free of Hfaca; this could be because the Hfaca layer is highly transparent. It was also noticed that the transmittance of the perovskite film with Hf3 was slightly lower than PCBM only, as shown in Fig. 2(b). This could be due to marginal increases in thickness of Hf3 from 8.9 nm to 11.7 nm. However, the difference is not significant compared to the control sample without any Hfaca layer.

The J–V curves showing the photovoltaic performance of the PSCs derived from several solution concentrations of Hfaca and without any Hfaca layer is shown in Fig. 3(a), and Table I shows the major device characteristics. It is observed that the PCBM/Ag control device has a PCE of 8.86%, an open-circuit voltage (Voc) of 0.788 V, a short-circuit current density (Jsc) of 20.38 mA/cm^2, and a fill factor (FF) of 55.20%. It is observed that the device made with a buffer layer of 1.0 mg/ml or Hf2 has the best PCE of 12.23%, Voc of 0.775 V, Jsc of 22.07 mA/cm^2, and FF of 71.00%. Devices with Hf1 and Hf3 as the buffer layer have a PCE of 11.53% and 11.52%, respectively. The PCEs of devices with Hfaca as the buffer layer greatly exceed those of the control device without the Hfaca layer. There was not much difference in the PCEs of devices prepared with varying concentrations of Hfaca as the buffer layer. However, the PCE of the devices with Hfaca as the buffer layer marginally increase with an increase in the concentration of Hfaca until the

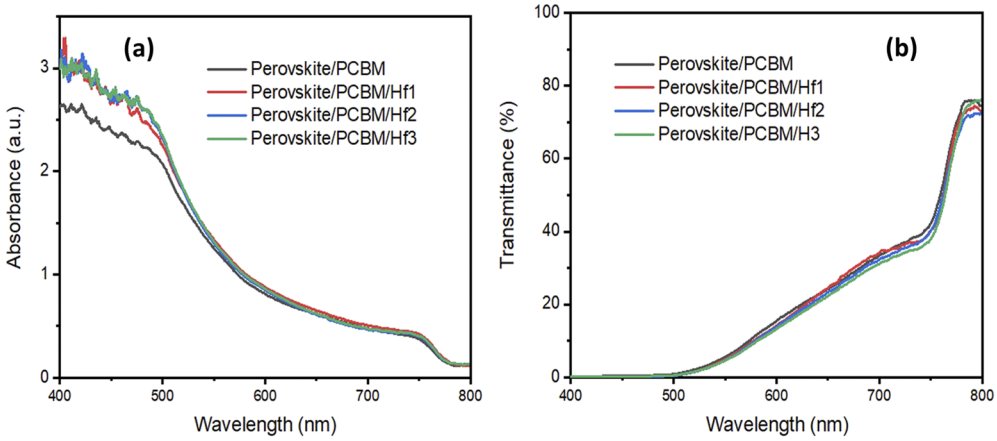

FIG. 2. (a) Absorbance and (b) transmittance spectra of various concentrations of the Hfaca layer and the control.

optimal concentration of 1.0 mg/ml or Hf2; beyond this point, the PCE value decreases. The improved Jsc and FF for devices fabricated with Hfaca as the buffer layer could be due to decreased contact barrier and an improved charge collection at the interface of PCBM/Ag when the Hfaca buffer layer is incorporated, which can prevent direct contact between the PCBM layer and the Ag layer, leading to an improved interface of good Ohmic contact. Increasing the concentration means increasing the thickness of the Hfaca buffer

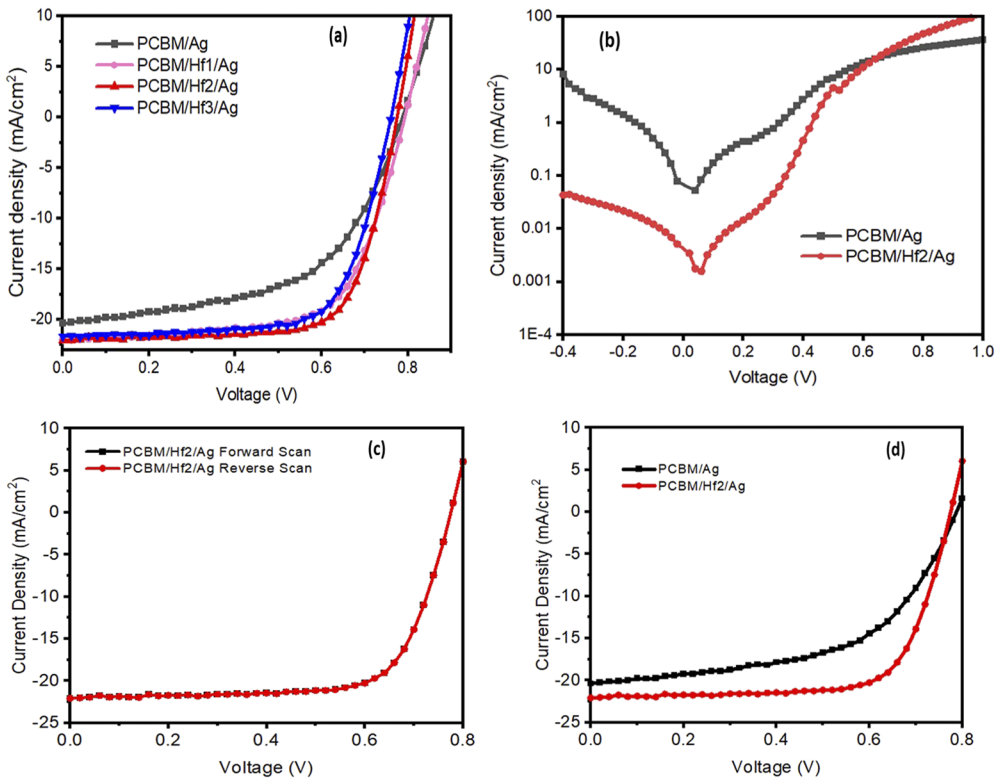

FIG. 3. (a) J–V characteristics for the inverted planner perovskite solar cells with different concentrations of Hfaca and without Hfaca, (b) J–V characteristics of perovskite/PCBM/Hf2/Ag under different scan directions, (c) the semi-logarithmic plots of dark J–V characteristics for the inverted planner perovskite solar cells with Hfaca and without Hfaca, and (d) J–V characteristics of the device with Hfaca and without Hfaca.

TABLE I. Photovoltaic properties for the inverted planar perovskite solar cells with different concentrations of Hfaca and without any Hfaca buffer layer.

Devices	V_{oc} (V)	J_{sc} (mA/cm^2)	FF (%)	PCE (%)
PCBM/Ag	0.788	20.38	55.20	8.86
PCBM/Hf1/Ag	0.793	22.00	66.01	11.53
PCBM/Hf2/Ag	0.775	22.07	71.00	12.23
PCBM/Hf3/Ag	0.740	22.32	69.90	11.52

layer. It was observed that an increase in the concentration of Hfaca had no appreciable effect on the performance of the PSCs; this provides the opportunity of choosing a wide range of concentration between 0.5 mg/ml and 1.5 mg/ml when preparing the Hfaca solution for buffer layer applications in PSCs. The main improvement in the performances of the devices with the Hfaca buffer layer comes from the improvement in Jsc and FF.

The semi-logarithmic plots of the dark J–V characteristics shown in Fig. 3(b) was presented to further illustrate the influence of the Hfaca buffer layer on the photovoltaic performance of inverted planar PSCs. The improvement in the FF is obtained mostly from the decrease in the leakage current of the PCBM/Hfaca/Ag-based device compared to the PCBM/Ag control device, as determined from Fig. 3(a). The decreased leakage current within the devices signifies better hole-blocking abilities when including the Hfaca buffer layer. This is as a result of the outstanding layer formation which leads to an excellent reduction in charge recombination within the device. This reduction effect is consistent with similar previous work.[24,32]

The abnormal hysteresis in the J–V curves has proven to be a major challenge in evaluating TiO_2-based n-i-p PSCs under different scan directions; however, this effect can be prevented if a p-i-n structure is used. Figure 3(c) represents the perovskite/PCBM/Hf2/Ag device under different scanning directions. The forward and reverse scanning directions for the device prepared with PCBM/Hf2/Ag show no hysteresis effect. The cause of the absence of the hysteresis effect in our devices and other devices prepared from other groups employing the inverted planar structure could be due to ion migration and the trap de-trapping process.[17,33] For the inverted p-i-n devices, the PCBM deposited on the perovskite layer can penetrate into the grain boundary (GB) of the perovskite film to prevent the charge trap state at the interfaces and reduce the ion migration along GBs of the perovskite layer, thereby leading to an efficient contribution to the reduction of the hysteresis, which is in agreement with similar previous research work.[17,32–34]

Figure 3(d) shows the J–V curves of PSCs fabricated from the control device without Hfaca (PCBM/Ag) and the device with optimized Hfaca (PCBM/Hf2/Ag). The J–V curves showed that the superior performance of the PSCs with the Hfaca buffer layer is mainly due to the improved values of Jsc and the FF.

The efficiency box plot from 15 devices shown in Fig. 4 (a) indicates that the device derived from a concentration of 1.0 mg/ml or PCBM/Hf2/Ag performed statistically better than devices derived from other solution concentrations of 0.5 mg/ml and 1.5 mg/ml as well as the control device (PCBM/Ag). It is also observed that devices made with hafnium acetylacetonate as the buffer layer performed better in terms of the power conversion efficiency than the control device without hafnium acetylacetonate as a buffer layer. The devices with Hfaca also show better reproducibility than the device without Hfaca. The reason for the improved repeatability with devices fabricated with Hfaca as the buffer layer could be because the Hfaca layer protects the PCBM layer from direct contact with the hot Ag electrode that will be deposited directly on the PCBM layer, which has the tendency of being corrosive to the PCBM layer and can create direct contact between the electrode and the absorber layer, which can lead to an increase in the leakage current of the device.

The photovoltaic performance of the devices was measured once daily to investigate the use of the Hfaca buffer layer for improving the stability of PSCs; the stability of the PSC devices fabricated from different concentrations of Hfaca and the control device without Hfaca (PCBM/Ag) was measured in a nitrogen-filled glove-box, as shown in Fig. 4(b). The devices with the Hfaca buffer layer show better stability, maintaining over 89% of the initial values of the PCE for all the concentrations after being stored in a nitrogen-filled glove-box for 15 days, while the control device without any Hfaca

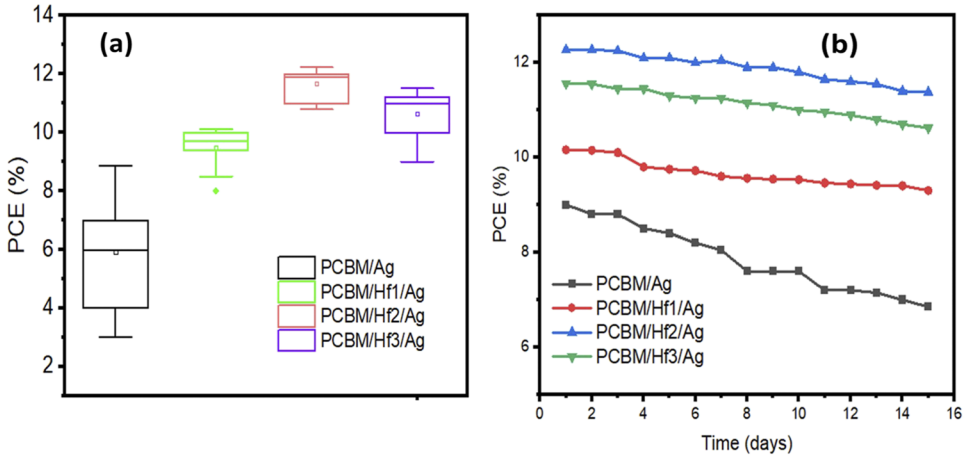

FIG. 4. (a) Statistical performance of all the devices fabricated, (b) stability of devices fabricated with the PCBM/Ag control device and devices fabricated with different concentrations of Hfaca.

buffer layer (PCBM/Ag) retains about 70% of its initial value of PCE after 15 days of storage in the nitrogen filled-glove box. Employing Hfaca as a buffer layer between the PCBM and Ag improves the stability of the device greatly. Also, the Hfaca buffer layer serves as a barrier that prevents the hot metal atoms from diffusing into the electron transport layer during thermal evaporation of the Ag electrode. These hot metal atoms could also affect the stability of the perovskite device without the Hfaca buffer layer, leading to thermal degradation. The results reveal that Hfaca could be one of the promising buffer layer materials for improving the stability of PSCs.

IV. CONCLUSION

In summary, it was observed that varying the concentration of the Hfaca buffer layer between 0.5 mg/ml and 1.5 mg/ml has no appreciable impact on the photovoltaic performance of PSCs. The superior performance of the devices with an Hfaca layer occurs mainly because of the improvement in Jsc and the FF; the improved Jsc and FF are due to the decreased contact barrier and an improved charge collection at the interface of PCBM/Ag of the devices with the Hfaca layer. The optimized concentration is found to be 1.0 mg/ml, with a corresponding PCE of 12.23. The study also reveals that incorporating Hfaca as a buffer layer leads to superior stability, retaining about 90% of its original PCE values after 15 days storage in the glove box, compared to the control device which retains about 70% of the initial PCE value under the same storage condition.

ACKNOWLEDGMENTS

This study was sponsored by the Pan African Materials Institute (PAMI) (Grant No. AUST/PAMI/2015 5415-NG) through funding from the World Bank African Centers of Excellence Program, to whom the authors are greatly indebted.

DATA AVAILABILITY

The data that support the findings of this study are available from the corresponding author upon reasonable request.

REFERENCES

[1] G. Xing, N. Mathews, S. Sun, S. S. Lim, Y. M. Lam, M. Gratzel, S. Mhaisalkar, and T. C. Sum, Science **342**, 344 (2013).
[2] M. M. Lee, J. Teuscher, T. Miyasaka, T. N. Murakami, and H. J. Snaith, Science **338**, 643 (2012).
[3] H.-S. Kim, C.-R. Lee, J.-H. Im, K.-B. Lee, T. Moehl, A. Marchioro, S.-J. Moon, R. Humphry-Baker, J.-H. Yum, J. E. Moser, M. Gratzel, and N.-G. Park, Sci. Rep. **2**(1), 591 (2012).
[4] S. D. Stranks, G. E. Eperon, G. Grancini, C. Menelaou, M. J. P. Alcocer, T. Leijtens, L. M. Herz, A. Petrozza, and H. J. Snaith, Science **342**, 341 (2013).
[5] A. Kojima, K. Teshima, Y. Shirai, and T. Miyasaka, J. Am. Chem. Soc. **131**, 6050 (2009).
[6] NREL, 2019.
[7] Z. He, H. Wu, and Y. Cao, Adv. Mater. **26**, 1006 (2014).
[8] C. Chen, S. Zhang, S. Wu, W. Zhang, H. Zhu, Z. Xiong, Y. Zhang, and W. Chen, RSC Adv. **7**, 35819 (2017).
[9] H. Kanda, T. W. Kim, H. Segawa, and S. Ito, APL Mater. **7**, 031117 (2019).
[10] H. Tan, A. Jain, O. Voznyy, X. Lan, F. P. García de Arquer, J. Z. Fan, R. Quintero-Bermudez, M. Yuan, B. Zhang, Y. Zhao, F. Fan, P. Li, L. N. Quan, Y. Zhao, Z.-H. Lu, Z. Yang, S. Hoogland, and E. H. Sargent, Science **355**, 722 (2017).
[11] M.-H. Liu, Z.-J. Zhou, P.-P. Zhang, Q.-W. Tian, W.-H. Zhou, D.-X. Kou, and S.-X. Wu, Opt. Express **24**, A1349 (2016).
[12] L. Etgar, P. Gao, Z. Xue, Q. Peng, A. K. Chandiran, and B. Liu, J. Am. Chem. Soc. **134**, 17396 (2012).
[13] J. Min, Z.-G. Zhang, Y. Hou, C. O. Ramirez Quiroz, T. Przybilla, C. Bronnbauer, F. Guo, K. Forberich, H. Azimi, T. Ameri, E. Spiecker, Y. Li, and C. J. Brabec, Chem. Mater. **27**, 227 (2015).
[14] J. Burschka, N. Pellet, S.-J. Moon, R. Humphry-Baker, P. Gao, M. K. Nazeeruddin, and M. Grätzel, Nature **499**, 316 (2013).
[15] J. You, Z. Hong, Y. Yang, Q. Chen, M. Cai, T.-B. Song, C.-C. Chen, S. Lu, Y. Liu, H. Zhou, and Y. Yang, ACS Nano **8**, 1674 (2014).
[16] A. S. Yerramilli, Y. Chen, D. Sanni, J. Asare, N. D. Theodore, and T. L. Alford, Org. Electron. **59**, 107 (2018).
[17] Y. Shao, Z. Xiao, C. Bi, Y. Yuan, and J. Huang, Nat. Commun. **5**(1), 5784 (2014).
[18] B. Chen, M. Yang, S. Priya, and K. Zhu, J. Phys. Chem. Lett. **7**, 905 (2016).
[19] G. Garcia-Belmonte, K. Zhu, and S. Priya, J. Phys. Chem. Lett. **6**, 4693 (2015).
[20] C. Eames, J. M. Frost, P. R. F. Barnes, B. C. O. Regan, A. Walsh, and M. S. Islam, Nat. Commun. **6**, 7497 (2015).
[21] X. Yin, M. Que, Y. Xing, and W. Que, J. Mater. Chem. A **3**, 24495 (2015).
[22] D. M. Sanni, Y. Chen, A. S. Yerramilli, E. Ntsoenzok, J. Asare, S. A. Adeniji, O. V. Oyelade, A. A. Fashina, and T. L. Alford, Mater. Renewable Sustainable Energy **8**, 3 (2019).
[23] C. He, F. Zhang, X. Zhao, C. Lin, and M. Ye, Front. Phys. **6**, 99 (2018).
[24] A. S. Yerramilli, Y. Chen, A. Knight, B. Gogoi, L. Li, Y. Song, Y. Shen, and T. L. Alford, Sol. Energy Mater. Sol. Cells **200**, 109927 (2019).
[25] W. Chen, L. Xu, X. Feng, J. Jie, and Z. He, Adv. Mater. **29**, 1603923 (2017).
[26] L. Yu, Q. Li, Z. Shi, H. Liu, Y. Wang, B. Zhang, S. Dai, J. Lin, and Z. Tan, ACS Appl. Mater. Interfaces **8**, 432 (2015).
[27] U. Krishnan, M. Kaur, M. Kumar, and A. Kumar, J. Photonics Energy **9**, 1 (2019).
[28] A. B. Muñoz-García, F. Sannino, G. Vitiello, D. Pirozzi, L. Minieri, A. Aronne, P. Pernice, M. Pavone, and G. D'Errico, ACS Appl. Mater. and Interfaces **7**, 21627 (2015).
[29] W. Zhang, M. Saliba, D. T. Moore, S. K. Pathak, M. T. Hörantner, T. Stergiopoulos, S. D. Stranks, G. E. Eperon, J. A. Alexander-Webber, A. Abate, A. Sadhanala, S. Yao, Y. Chen, R. H. Friend, L. A. Estroff, U. Wiesner, and H. J. Snaith, Nat. Commun. **6**, 6142 (2015).
[30] Y. Chen, A. Yerramilli, Y. Shen, Z. Zhao, and T. Alford, Sol. Energy Mater. Sol. Cells **174**, 478 (2018).
[31] B. Ingham and M. F. Toney, *X-Ray Diffraction for Characterizing Metallic Films* (Woodhead Publishing Limited, 2014), Vol. 1.
[32] J. H. Kim, P.-W. Liang, S. T. Williams, N. Cho, C.-C. Chueh, M. S. Glaz, D. S. Ginger, and A. K.-Y. Jen, Adv. Mater. **27**, 695 (2015).
[33] J. W. Jung, C.-C. Chueh, and A. K.-Y. Jen, Adv. Mater. **27**, 7874 (2015).
[34] Y. Hou, W. Chen, D. Baran, T. Stubhan, N. A. Luechinger, B. Hartmeier, M. Richter, J. Min, S. Chen, C. O. R. Quiroz, N. Li, H. Zhang, T. Heumueller, G. J. Matt, A. Osvet, K. Forberich, Z.-G. Zhang, Y. Li, B. Winter, P. Schweizer, E. Spiecker, and C. J. Brabec, Adv. Mater. **28**, 5112 (2016).